5-2023

Reynolds-Averaged Navier-Stokes CFD Simulation of High-Speed Boundary Layers

Michael Tullis

REYNOLDS-AVERAGED NAVIER-STOKES CFD SIMULATION OF HIGH-SPEED BOUNDARY LAYERS

Michael Tullis
Student
University of Arkansas
Fayetteville, AR

Keith Walters
Research Advisor
University of Arkansas
Fayetteville, AR

ABSTRACT

This paper presents an investigation of Reynolds-averaged Navier-Stokes (RANS) turbulence models used in computational fluid dynamics (CFD) simulations of boundary layer flow and heat transfer in high Mach number flows. This study evaluates an industry standard RANS turbulence model (k-omega SST) and a recently proposed modification to that model (Danis and Durbin [1]), and quantifies the accuracy for predicting high Mach number boundary layer flow. The test cases were previously documented by Duan et al. (2018), who used direct numerical simulation (DNS) to calculate boundary layer flow of an ideal gas over a flat plate at freestream Mach numbers ranging from 2 to 14 and wall to recovery temperature ratios of 0.18 to 1. Boundary layer profiles were evaluated at two streamwise locations, one where the boundary layer height matched the DNS data and the second where the wall shear stress matched DNS data. Results show that the accuracy of RANS models degrades for high-speed regimes compared to incompressible or subsonic flow but that the compressibility correction factor [1] improves the results for some of the test cases.

Keywords: CFD, turbulence modeling, high-speed flow, boundary layers, RANS

NOMENCLATURE

M	Mach number, dimensionless
U_∞	Free stream velocity, $\frac{m}{s}$
ρ	Density, $\frac{kg}{m^3}$
k	Turbulent kinetic energy, $\frac{J}{kg}$
T_r	Recovery Temperature, K
T	Temperature, K
τ	Shear stress, Pa
δ	Boundary layer thickness, mm
Re_x	Reynolds number based on x-direction position downstream of plate leading edge
Re_δ	Reynolds number based on boundary layer thickness and freestream conditions
Re_τ	Reynolds number based on boundary layer thickness, shear velocity and wall viscosity
C_f	Skin friction coefficient

Subscripts

w	Wall variable
∞	Freestream variable

1. INTRODUCTION

Hypersonic flight regimes have long been relevant to high-speed aerospace systems such as reentry vehicles and ballistic missiles and are becoming more relevant as military and civilian applications, for these flight speeds are being considered in next-generation designs. As the technology that utilizes these speeds grows and matures, the need for more accurate and efficient computational simulations also grows. One key aspect of aerodynamic analysis is the calculation of the thermal and velocity boundary layer characteristics using computational fluid dynamics (CFD). The boundary layers dictate the frictional forces and frictional heating which relate to the drag and heat transfer on the vehicle. Currently the most common class of turbulence modeling for CFD analysis of high-speed systems is Reynolds-averaged Navier-Stokes (RANS) modeling. A well-known representative model is the two-equation k-ω shear stress transport (SST) model which is currently used for wide array of aerospace relevant CFD simulations [2]. Since this is a widely used model, it is important that results obtained from computational simulations using it are accurate.

Classical RANS models were primarily developed for use in relatively low-speed flow conditions, from incompressible up to moderately supersonic, and with no significant wall heat transfer effects. As a result, hypersonic and even supersonic flow speeds remain subject to significant levels of uncertainty due to the use of industry standard computational fluid dynamics turbulence models such as the k-ω SST model.

Research efforts are currently underway on several fronts to improve turbulence modeling capability for high-speed flow. This includes the use of scale-resolving methods such as wall-modeled large-eddy simulation (LES) or hybrid RANS-LES models. While both of these approaches are potentially more accurate than RANS modeling, they incur a substantial increase in computational cost. In the near term, modifications to RANS models that make them more accurate for high-speed applications are likely to produce valuable improvements in CFD capability that can be rapidly implemented into current analysis and design practice.

One identified weakness of current RANS turbulence models is that they utilize Morkovin's hypothesis [3], which has been found to be incorrect near the wall boundaries [1]. Specifically, the authors note that two-equation k-ω models applied to turbulent boundary layers tend to overpredict turbulent viscosity and underpredict mean velocity in the near-wall region when non-negligible wall heat transfer effects are present. More generally, the presence of compressible terms in the governing equations for turbulent statistical quantities, which

can be significant in high-speed flows but are neglected in most standard model forms, can lead to inaccurate predictions.

The objective of this work is to evaluate the performance of a standard model form, k-ω SST, for a simple high-speed boundary layer flow, as well as an improved model form proposed in [1]. The work serves as a baseline for comparison to other model forms that may be developed as part of future research. Validation is performed by comparison to recent work performed by Duan et al. [4] to compute hypersonic and supersonic flow regimes using direct numerical simulation (DNS) and to build a database of these results in order to provide accurate data for validation purposes. Published results from [4] include several test cases with Mach numbers ranging from 2.5 to 14 and wall to recovery temperature ratios ranging from 0.18 to 1.

2. MATERIALS AND METHODS

2.1 Simulation Details

For all simulations in this paper the open-source CFD software flowPsi was utilized. flowPsi is a density-based, ideal gas, finite-volume flow solver developed within the Loci framework. The two-dimensional domain consisted of a flat plate at the bottom boundary, with a short upstream symmetry condition to allow proper stagnation of the freestream flow at the leading edge. Supersonic freestream conditions were applied at the inlet plane, and uniform ambient pressure was applied at the outflow plane. A farfield boundary corresponding to the freestream conditions was applied at the top surface.

For the three lowest Mach number test cases a domain that extended 2 meters in the x-direction and 1 meter in the y-direction was used. For the two highest Mach number cases a larger extent in the x-direction was required in order to provide enough distance for the boundary layers to fully develop to the conditions documented in [4]. For these two cases the overall domain was lengthened to 20 meters. The smaller domain used for the lower Mach number test cases is shown in Fig. 1, with boundary condition locations indicated.

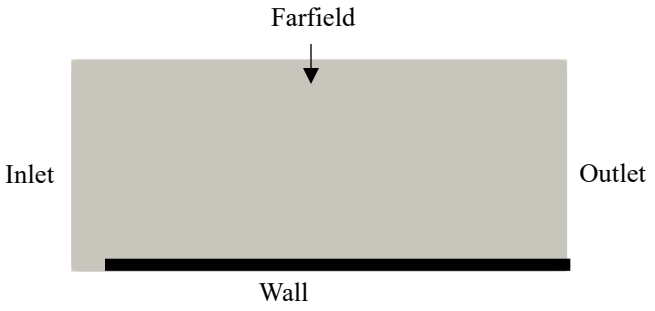

FIGURE 1: The full domain used for the lower Mach number test cases

A Cartesian structured mesh topology was used for this relatively simple flow geometry. In the near-wall region, high aspect ratio cells were used in order to accurately represent high variable gradients in the wall-normal (y) direction. Likewise, stretching in the y-direction was used in order to cluster cells close to the wall. The first cell mesh size was selected to ensure that the y^+ value was less than one, which was verified for all cases after the simulations were completed. A view of the full mesh is shown in Fig. 2, the grid refinement can be seen near the inflow and the wall.

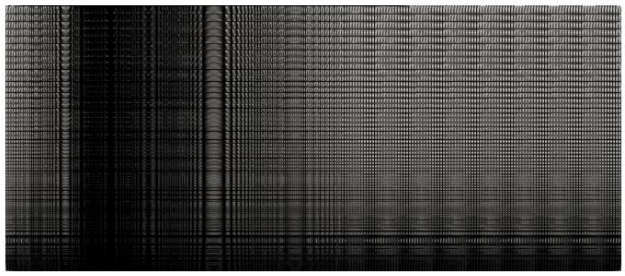

FIGURE 2: A full view of the mesh

In order to reproduce the conditions of the DNS validation test cases, air was used as the working fluid and Sutherlands law was used to compute dynamic viscosity for all cases except for the M8Tw048 case. For this case the working fluid was Nitrogen and Keyes law was used to compute viscosity. A user-defined module was developed in Loci to implement Keyes law for this case instead of using Sutherland's law.

All cases were run using an implicit solution method with first-order temporal advancement until a steady-state condition was reached. The HLLC scheme [5] was used to discretize the advective terms with second-order accurate spatial reconstruction of face states. Second-order differencing was used for all diffusive terms.

2.2 Test Case Description

Five separate test cases were run, each corresponding to specific freestream and wall conditions used in [4]. The test case conditions are summarized in Table 1. For each test case, two simulations were performed, one using a standard form of the k-ω SST model [2] and one using the k-ω SST model with the proposed Danis and Durbin compressibility correction factor [1]. In general, because the CFD results did not match the DNS data for all quantities of interest, it was not possible to compare results at a location where all relevant dimensionless quantities (e.g. Re_x, Re_δ, Re_τ, C_f) were equal. Likewise, results could not be prepared at equal dimensional streamwise locations, because the DNS study used recycling boundary conditions to simulate only part of the boundary layer region, and no physical x-location was explicitly defined. In the present study, in an attempt to make the most valid comparison possible, results were analyzed at two different locations, one corresponding to the location where the 99% boundary layer thickness was the same as in the DNS, and the second to where the wall shear stress was the same. The values for these two quantities for each case are shown in Table 2.

Table 1: Freestream and wall temperature conditions of the test cases

Case	M_∞	U_∞,$\frac{m}{s}$	ρ_∞,$\frac{kg}{m^3}$	T_∞,K	T_w,$\frac{m}{s}$	$\frac{T_w}{T_r}$
M2P5	2.5	823.6	0.100	270.0	568.0	1.0
M6Tw025	5.84	869.1	0.044	55.2	97.5	0.25
M6Tw076	5.86	870.4	0.043	55.0	300.0	0.76
M8Tw048	7.87	1155.1	0.026	51.8	298.0	0.48
M14Tw018	13.64	1882.2	0.017	47.4	300.0	0.18

Table 2: Boundary layer thickness and wall shear stress used for analysis per each test case

Case	δ,mm	τ_w,Pa
M2P5	7.7	79.6
M6Tw025	3.6	27.9
M6Tw076	23.8	16
M8Tw048	35.2	12.9
M14Tw018	66.1	12

3. RESULTS AND DISCUSSION

For each model and test case comparison was made between the CFD results and DNS data for two different mean flow variables, velocity and temperature. Therefore for each case and model combination two different plots are presented, with three different curves on each plot. The different plots represent the different ways that the data was analyzed and collected, the solid line labeled DNS correlates to the data from the DNS database. The dotted line plot labeled Comparison 1 is the data corresponding to the x location where the boundary layer thickness was the same as what was reported in the DNS database. The dashed line plot labeled Comparison 2 is the data corresponding to the x location where the wall shear stress is equal to that found in the DNS database. After all mean velocity temperature results are presented, a discussion follows.

3.1 k-ω SST Model Results

Results are first presented for the unmodified standard form of the k-ω SST model. These are shown in Figs. 3-12. As the figures show, the k-ω SST can be seen to be a relatively inaccurate model as the Mach number is increased. Overall, the model does perform better at predicting the mean velocity than it does at being able to correctly predict the mean temperature. Also, the plots located where the boundary layer thickness was the same as the DNS value (Comparison 1) seems to match the overall profile shape much more accurately than the plot where the wall shear stress was the same. In the M2P5 case there is relatively good agreement with the k-ω SST model and the DNS data, this is due to it being a slightly lower speed flow and closer to the conditions for which most two-equation models have been previously calibrated and validated. The disagreement in the results as Mach number increases, however, highlights the inherent uncertainty for this class of model and suggests that they must be used with great care in high-speed applications.

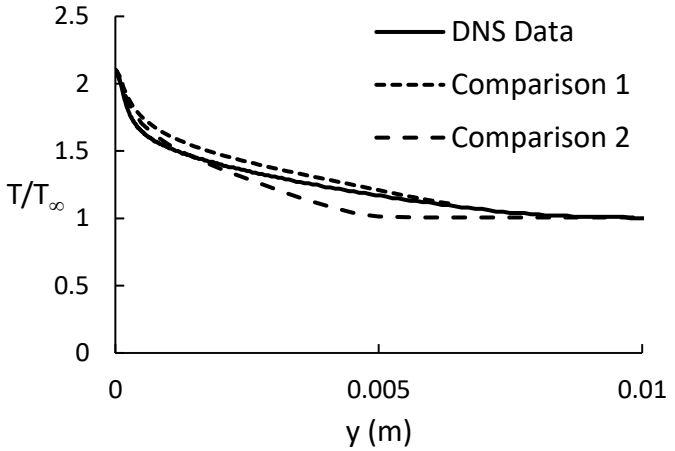

FIGURE 3: Plot of mean temperature versus wall-normal distance for the M2P5 case and standard k-ω SST turbulence model. Comparison 1 is taken at a streamwise location at which the boundary layer thickness is equal to the DNS value, and Comparison 2 is taken at a streamwise location at which the wall shear stress is equal to the DNS value.

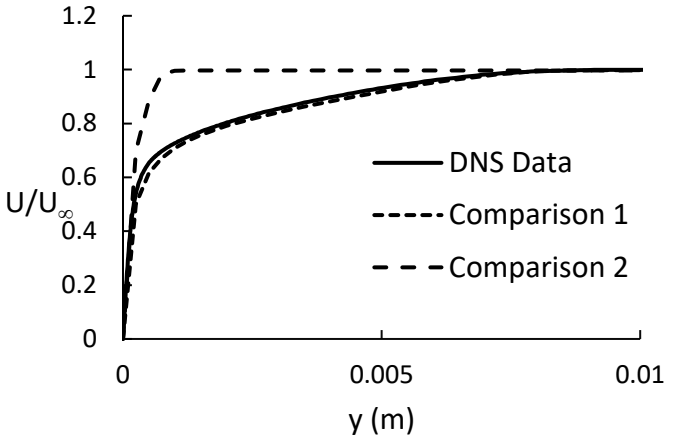

FIGURE 4: Plot of mean streamwise velocity versus wall-normal distance for the M2P5 case and standard k-ω SST turbulence model. Curve locations as in Fig. 3.

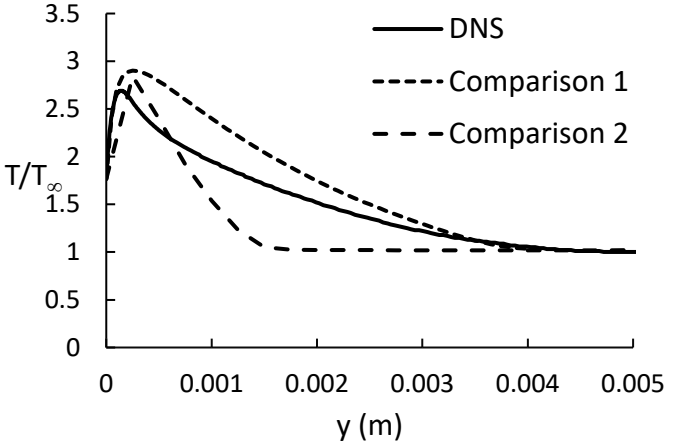

FIGURE 5: Plot of mean temperature versus wall-normal distance for the M6Tw025 case and standard k-ω SST turbulence model. Curve locations as in Fig. 3.

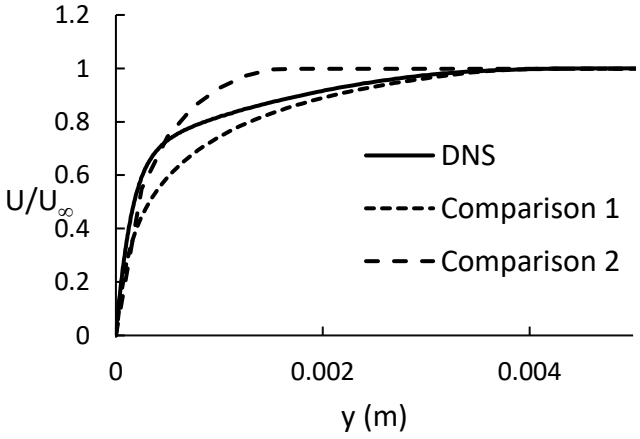

FIGURE 6: Plot of mean streamwise velocity versus wall-normal distance for the M6Tw025 case and standard k-ω SST turbulence model. Curve locations as in Fig. 3.

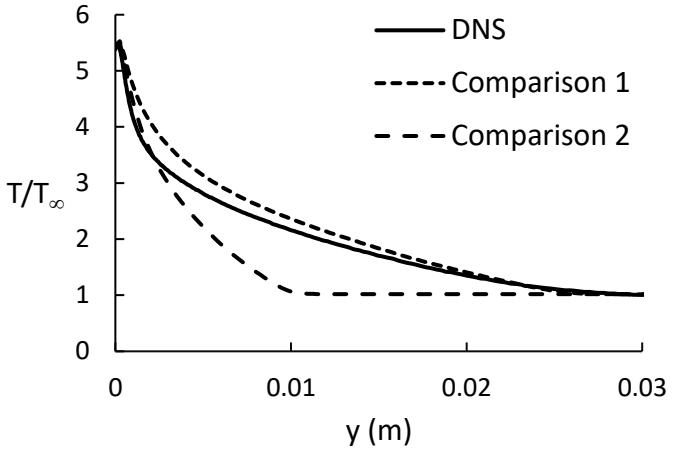

FIGURE 7: Plot of mean temperature versus wall-normal distance for the M6Tw076 case and standard k-ω SST turbulence model. Curve locations as in Fig. 3.

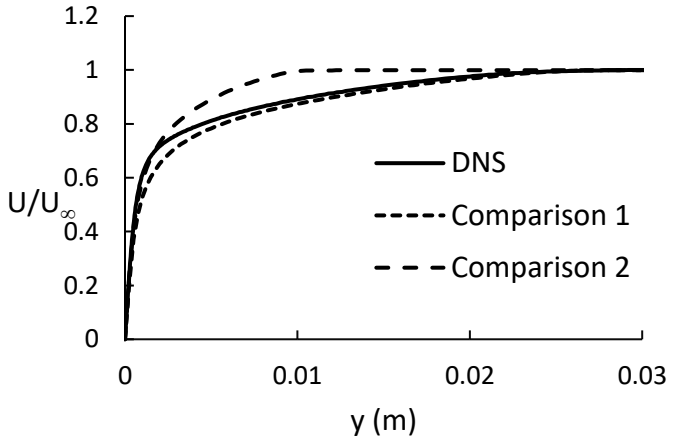

FIGURE 8: Plot of mean streamwise velocity versus wall-normal distance for the M6Tw076 case and standard k-ω SST turbulence model. Curve locations as in Fig. 3.

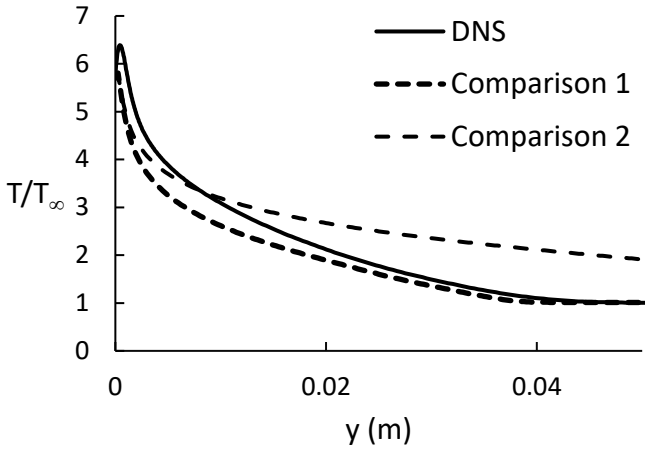

FIGURE 9: Plot of mean temperature versus wall-normal distance for the M8Tw048 case and standard k-ω SST turbulence model. Curve locations as in Fig. 3.

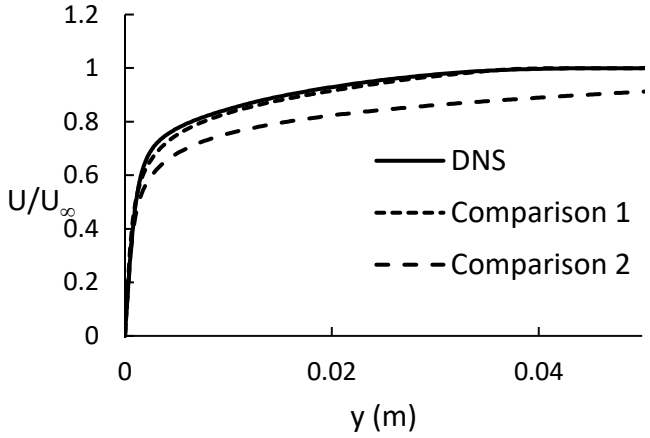

FIGURE 10: Plot of mean streamwise velocity versus wall-normal distance for the M8Tw048 case and standard k-ω SST turbulence model. Curve locations as in Fig. 3.

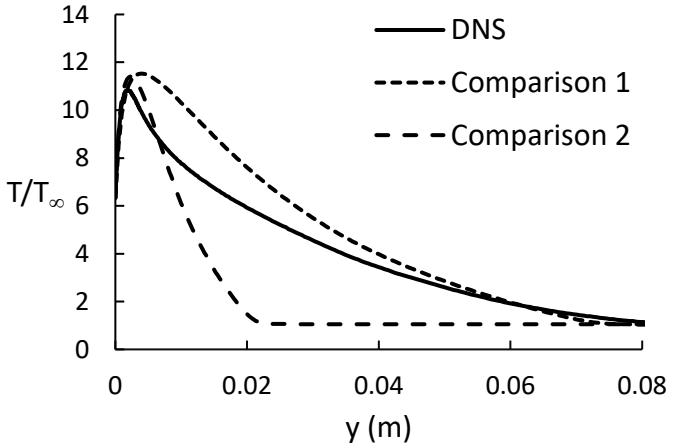

FIGURE 11: Plot of mean temperature versus wall-normal distance for the M14Tw018 case and standard k-ω SST turbulence model. Curve locations as in Fig. 3.

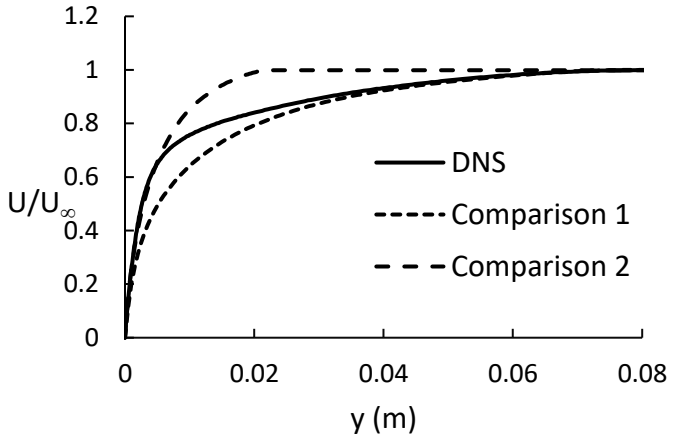

FIGURE 12: Plot of mean streamwise velocity versus wall-normal distance for the M14Tw018 case and standard k-ω SST turbulence model. Curve locations as in Fig. 3.

3.2 Danis and Durbin corrected model

In order to evaluate the Danis and Durbin [1] compressibility correction factor, a Loci module was developed and implemented into the flowPsi solver. Results using the corrected model for the same test cases presented in section 3.1 are shown in Figs. 13-22. The correction factor can be seen to improve overall agreement with the DNS data. The improvements can be seen primarily near the surface for both the mean temperature and velocity. The improvement seems less significant for the Mach 14 case where the overall agreement of the data is much lower than for the other cases. Overall, however, it can be stated that the compressibility correction factor improves agreement with the DNS data, more noticeably near the wall. The results support the conclusion that empirical correction factors for traditional two-equation models can be developed and used with success, although significant uncertainty remains and even corrected models must be used with caution.

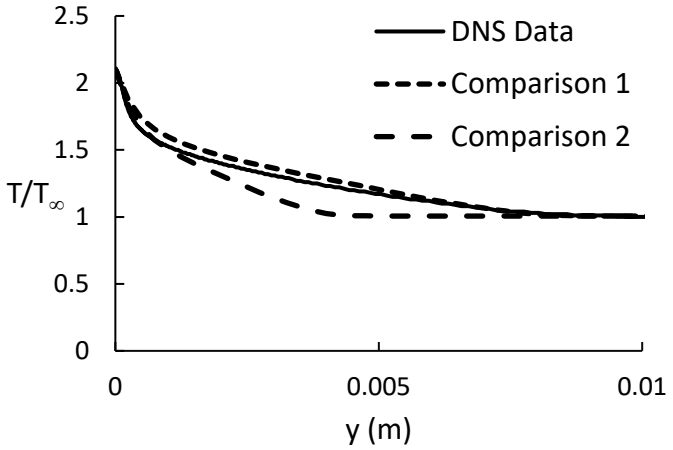

FIGURE 13: Plot of mean temperature versus wall-normal distance for the M2P5 case and compressibility corrected k-ω SST turbulence model. Comparison 1 is taken at a streamwise location at which the boundary layer thickness is equal to the DNS value, and Comparison 2 is taken at a streamwise location at which the wall shear stress is equal to the DNS value.

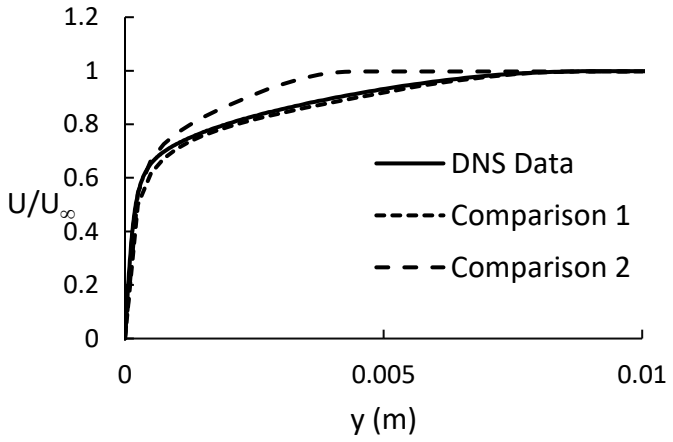

FIGURE 14: Plot of mean streamwise velocity versus wall-normal distance for the M2P5 case and compressibility corrected k-ω SST turbulence model. Curve locations as in Fig. 3.

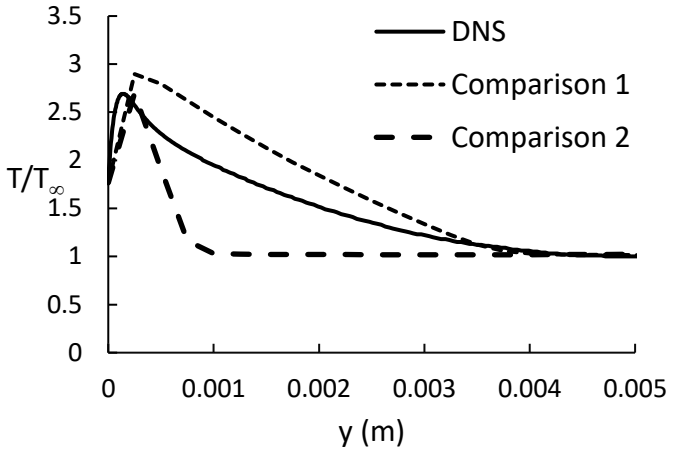

FIGURE 15: Plot of mean temperature versus wall-normal distance for the M6Tw025 case and compressibility corrected k-ω SST turbulence model. Curve locations as in Fig. 3.

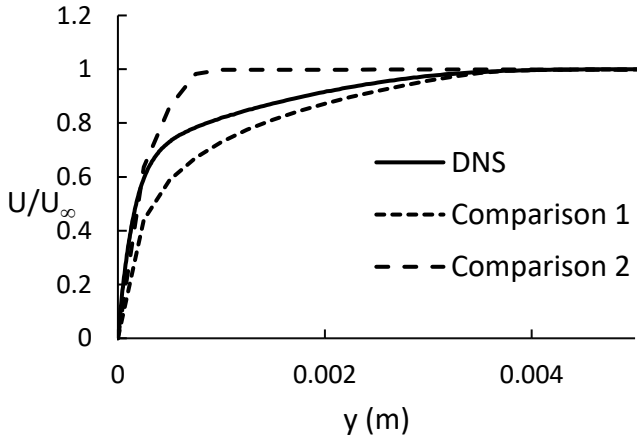

FIGURE 16: Plot of mean streamwise velocity versus wall-normal distance for the M6Tw025 case and compressibility corrected k-ω SST turbulence model. Curve locations as in Fig. 3.

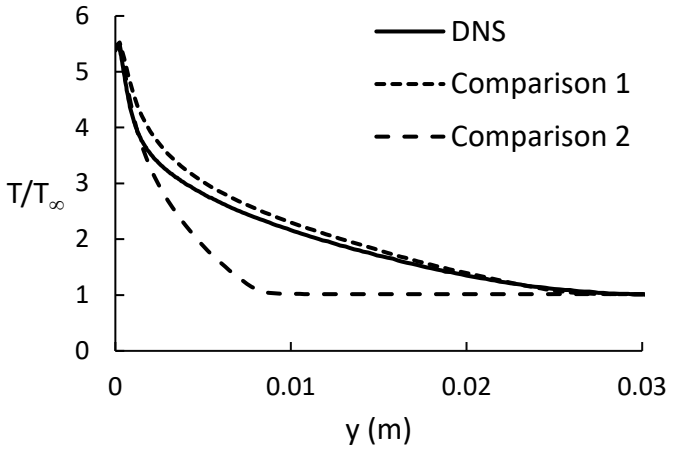

FIGURE 17: Plot of mean temperature versus wall-normal distance for the M6Tw076 case and compressibility corrected k-ω SST turbulence model. Curve locations as in Fig. 3.

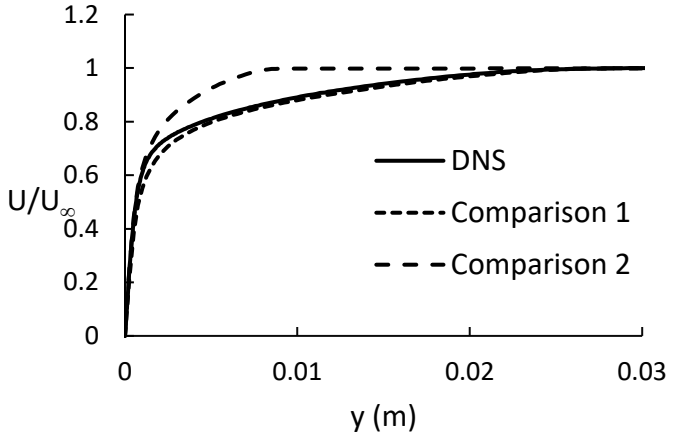

FIGURE 18: Plot of mean streamwise velocity versus wall-normal distance for the M6Tw076 case and compressibility corrected k-ω SST turbulence model. Curve locations as in Fig. 3.

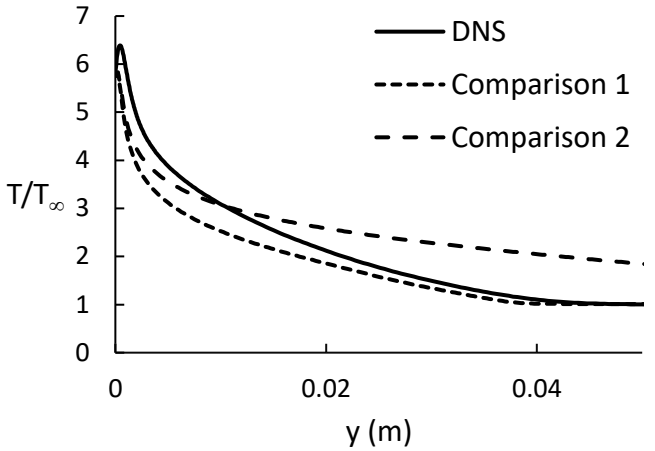

FIGURE 19: Plot of mean temperature versus wall-normal distance for the M8Tw048 case and compressibility corrected k-ω SST turbulence model. Curve locations as in Fig. 3.

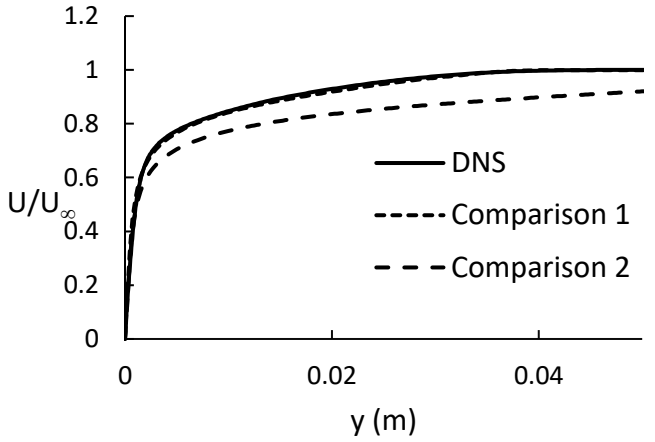

FIGURE 20: Plot of mean streamwise velocity versus wall-normal distance for the M8Tw048 case and compressibility corrected k-ω SST turbulence model. Curve locations as in Fig. 3.

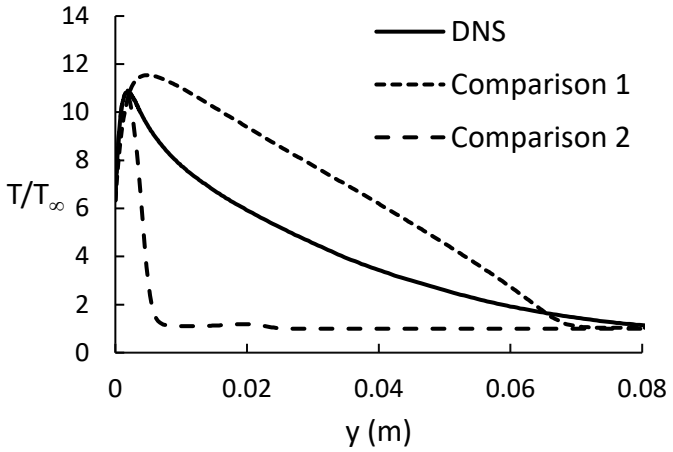

FIGURE 21: Plot of mean temperature versus wall-normal distance for the M14Tw018 case and compressibility corrected k-ω SST turbulence model. Curve locations as in Fig. 3.

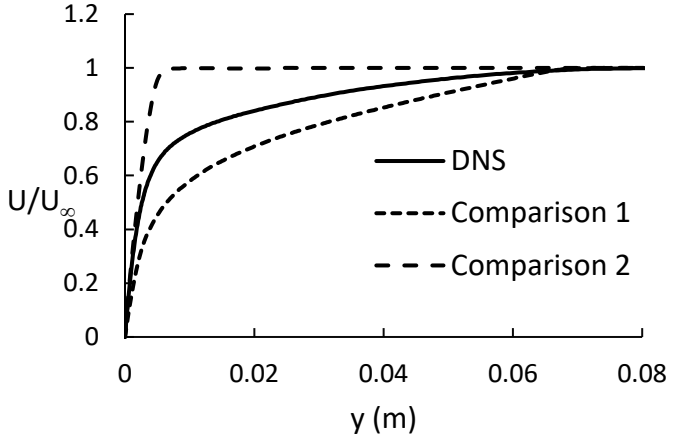

FIGURE 22: Plot of mean streamwise velocity versus wall-normal distance for the M14Tw018 case and compressibility corrected k-ω SST turbulence model. Curve locations as in Fig. 3.

3.3 Comparison of the standard k-ω SST model to the Danis and Durbin compressibility correction factor

For the majority of the test cases the compressibility correction factor presented by Danis and Durbin [1] mitigated errors near the wall and produced more accurate results in the near wall region for the high-speed flow regimes. This is most evident in the mean velocity results, while the mean temperature results appear to show less significant improvement. This can be seen most clearly for the M8Tw048 case, both models are unable to predict the temperature spike near the wall and as a result underestimate the temperature of the fluid near the wall and as the freestream is approached. Additionally, both models seem to yield higher errors in temperature prediction anytime whenever there is a maximum temperature off the wall and a change in sign of the temperature gradient. This is caused by the wall temperature $\frac{T_w}{T_r}$ being lower, resulting in non-negligible heat transfer near the wall and causing the issues with Morkovins hypothesis to become more evident. When comparing the plots for the lower $\frac{T_w}{T_r}$ cases it appears that the k-ω SST may even slightly outperform the Danis and Durbin compressibility correction factor, though this can likely be addressed through further model refinement.

One interesting exception to the general overall trend is that for the M14Tw018 case the standard k-ω SST model appears outperform the compressibility corrected model with respect to both the mean temperature and mean velocity. This difference is more clearly visible in the mean velocity plot.

3.4 Effect of the compressibility correction factor

The compressibility correction introduced in [1] modifies the production and destruction terms in the transport equation for specific dissipation rate. The transport equations for the k-ω SST model in stationary flow are:

$$\frac{\partial(\rho u_j k)}{\partial x_j} = P - \beta^* \rho k \omega + \frac{\partial}{\partial x_j}\left[(\mu + \sigma_k \mu_T)\frac{\partial k}{\partial x_j}\right]$$

$$\frac{\partial(\rho u_j \omega)}{\partial x_j} = f\gamma \frac{\omega}{k} P - f\beta\rho\omega^2 + \frac{\partial}{\partial x_j}\left[(\mu + \sigma_\omega \mu_T)\frac{\partial \omega}{\partial x_j}\right] + 2(1 - F_1)\sigma_{\omega 2}\frac{\rho}{\omega}\frac{\partial k}{\partial x_j}\frac{\partial \omega}{\partial x_j}$$

The value of the compressibility function, *f*, is prescribed by a function defined in [1], and limits to 1 as Ma $\rightarrow$ 0 and wall-to-recovery temperature ratio $\frac{T_w}{T_r} \rightarrow 1$. The model is thus sensitized to the effects of both high velocity and the temperature gradients that arise in supersonic flow conditions. Near the wall the correction function reduces the magnitude of the source terms in the ω equation. Throughout the bulk of the boundary layer it increases or decreases the source term contribution depending on the flow parameters for the particular test case. Overall, the turbulent kinetic energy is not altered very much, however in the two cases with the lowest wall-to-recovery temperature ratio it can be seen that the turbulent kinetic energy for the corrected model varies greatly from the standard model. For the M14Tw018 case this effect can be see far into the boundary layer while in the M6Tw025 case the effect is just a shorter peak.

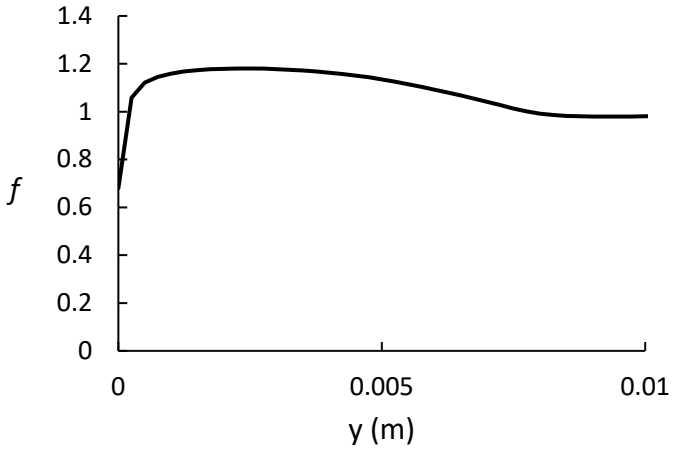

FIGURE 23: Boundary layer profile of the compressibility correction function *f* for the M2P5 test case.

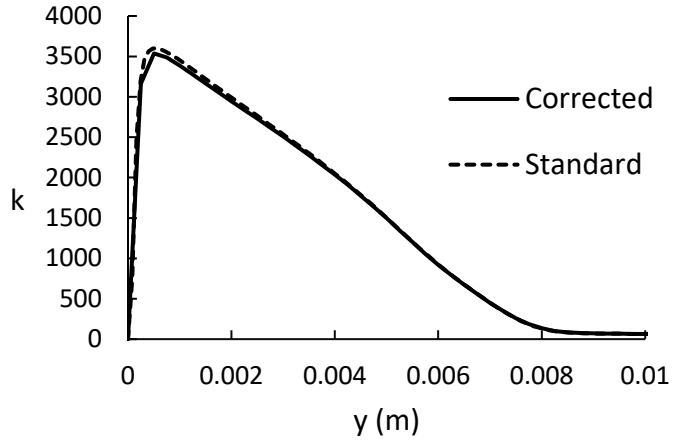

FIGURE 24: Boundary layer profiles of turbulent kinetic energy using standard and corrected SST models, for the M2P5 test case.

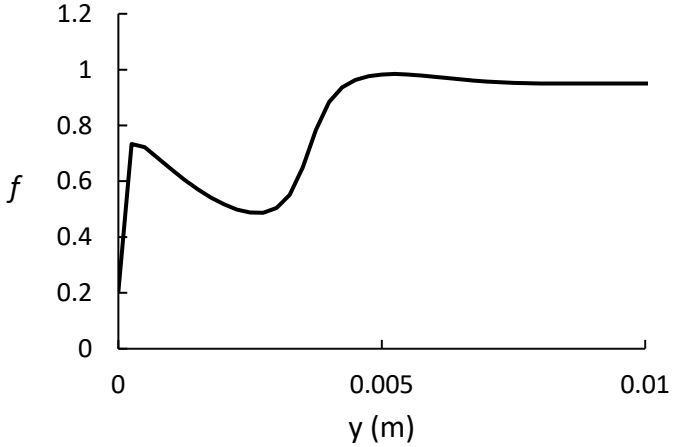

FIGURE 25: Boundary layer profile of the compressibility correction function *f* for the M6Tw025 test case.

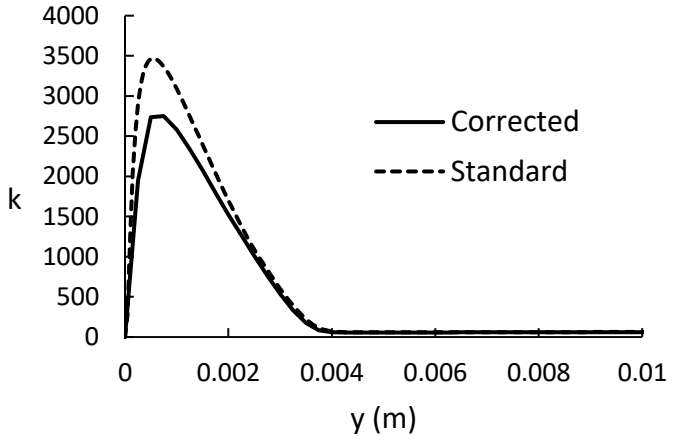

FIGURE 26: Boundary layer profiles of turbulent kinetic energy using standard and corrected SST models, for the M6Tw025 test case.

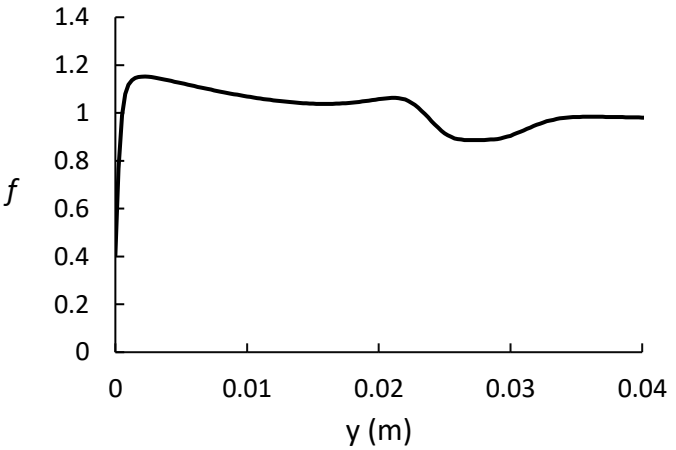

FIGURE 27: Boundary layer profile of the compressibility correction function *f* for the M6Tw076 test case.

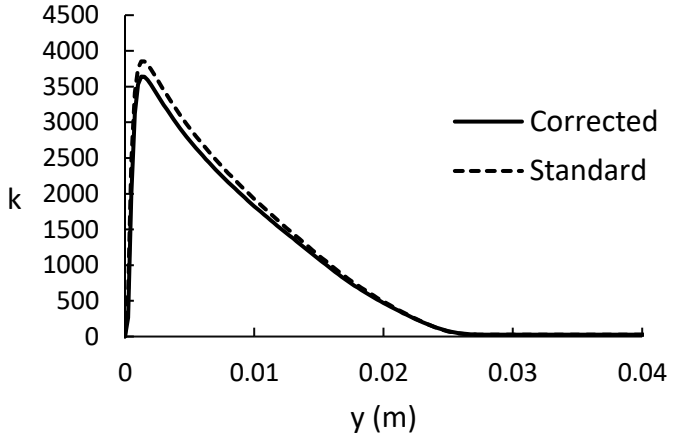

FIGURE 28: Boundary layer profiles of turbulent kinetic energy using standard and corrected SST models, for the M6Tw076 test case.

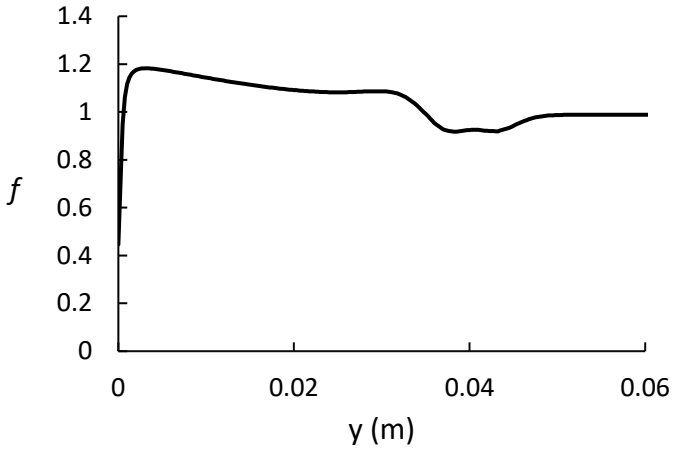

FIGURE 29: Boundary layer profile of the compressibility correction function *f* for the M8Tw048 test case.

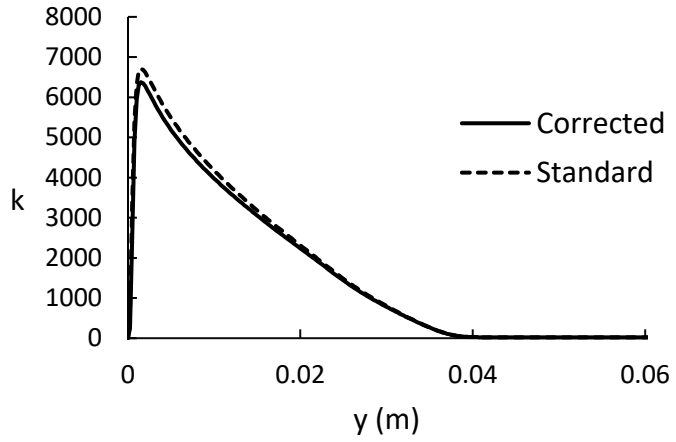

FIGURE 30: Boundary layer profiles of turbulent kinetic energy using standard and corrected SST models, for the M8Tw048 test case.

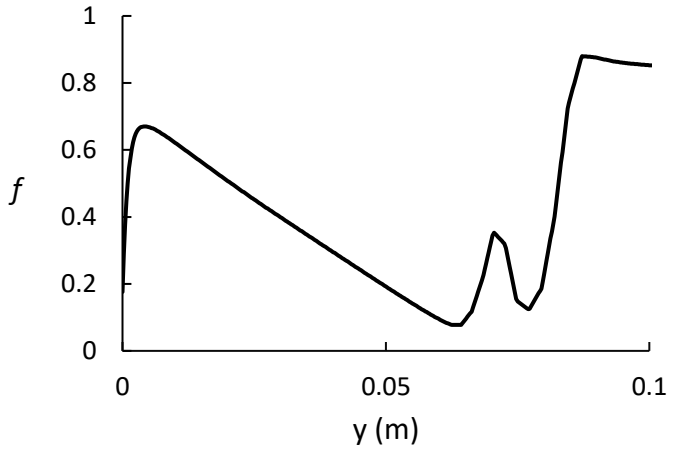

FIGURE 31: Boundary layer profile of the compressibility correction function *f* for the M14Tw018 test case.

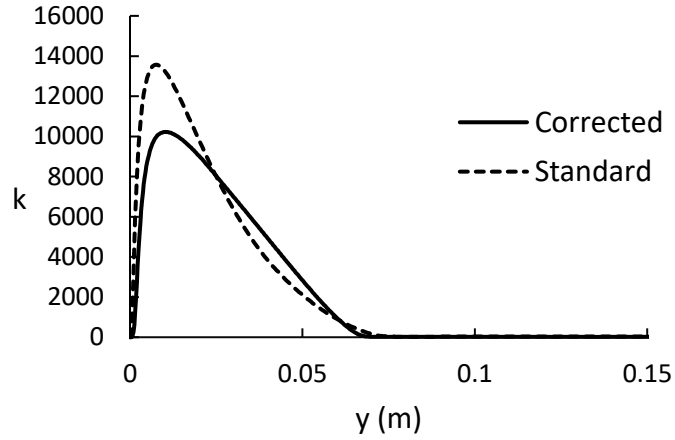

FIGURE 32: Boundary layer profiles of turbulent kinetic energy using standard and corrected SST models, for the M14Tw018 test case.

4. CONCLUSION

Results obtained with the standard form of the k-ω SST model show significant error when compared to the DNS data, especially at higher Mach numbers. This supports the conclusion of previous researchers that the Morkovin [3] hypothesis does introduce significant error into the k-ω model. It is shown that for moderate Mach number and temperature ratio $\left(\frac{T_w}{T_r}\right)$ the Danis and Durbin [1] compressibility correction factors improves the underlying k-ω model, in this case the SST version. However, for the highest Mach number and in cases with low $\frac{T_w}{T_r}$ the underlying compressibility correction factor is less effective and may even lead to slightly less accurate results. Overall, the results suggest that the approach taken in [1], i.e. the use of relatively simple modifications to baseline models to account for compressibility effects, is a valid alternative to more advanced modeling methods such as large-eddy simulation. The model in [1] appears to therefore be a step in the right direction. The

inclusion of additional test cases into the set used for model calibration, and the investigation of different forms for modification functions may lead to further improvements in the future to RANS-based eddy-viscosity modeling in high-speed flows.

ACKNOWLEDGEMENTS

This work could not have been done without the help of Dr. Keith Walters, as his guidance has been fundamental to the completion of this research and subsequent paper. I would also like to thank Dr. Jim Leylek for his contributions and guidance through the course of the research and writing of the paper, his continued support and guidance was crucial to the completion of the paper. The AHPCC has been a key component in the completion of this work, without them and the resources they provide this work would not have been able to have been completed.

REFERENCES

[1] Danis, Mustafa E., and Paul Durbin. "Compressibility Correction to K−ω Models for Hypersonic Turbulent Boundary Layers." *AIAA Journal* 60, no. 11, 2022, 6225–34. https://doi.org/10.2514/1.j062027.

[2] Menter, F. R., "Two-Equation Eddy-Viscosity Turbulence Models for Engineering Applications," AIAA Journal, Vol. 32, No. 8, 1994, pp. 1598–1605. https://doi.org/10.2514/3.12149

[3] Morkovin, M. V., "Effects of Compressibility on Turbulent Flows," Mécanique de la Turbulence, edited by A. J. Favre, CNRS, Paris, 1962, pp. 367–387.

[4] Zhang, C., Duan, L., and Choudhari, M. M., "Direct Numerical Simulation Database for Supersonic and Hypersonic Turbulent Boundary Layers," AIAA Journal, Vol. 56, No. 11, 2018, pp. 4297–4311. https://doi.org/10.2514/1.J057296

[5] Toro, E. F., M. Spruce, and W. Speares. "Restoration of the Contact Surface in the HLL-Riemann Solver." *Shock Waves* 4, no. 1 (1994): 25–34. https://doi.org/10.1007/bf01414629.